Title
MEAN SQUARE DISPLACEMENT OF SURFACE ATOMS ON THE SILICON (111) CRYSTAL FACE

Author
Crump, James Grace.

Publication Date
1975-03-01

LBL-3575

MEAN SQUARE DISPLACEMENT OF SURFACE ATOMS ON THE SILICON (111) CRYSTAL FACE

James Grace Crump
(M. S. thesis)

March 1975

Prepared for the U. S. Energy Research and
Development Administration under Contract W-7405-ENG-48

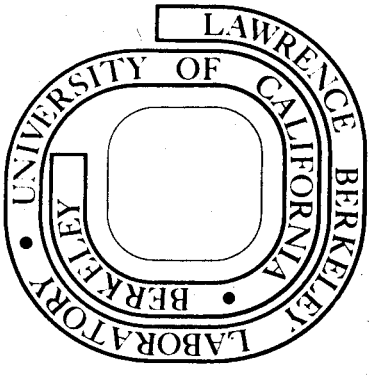

LBL-3575

DISCLAIMER

MEAN SQUARE DISPLACEMENT OF SURFACE ATOMS
ON THE SILICON (111) CRYSTAL FACE

Contents

MEAN SQUARE DISPLACEMENT OF SURFACE ATOMS ON THE SILICON (111) CRYSTAL FACE

James Grace Crump

Inorganic Materials Research Division, Lawrence Berkeley Laboratory and Department of Chemistry; University of California, Berkeley, California 94720

ABSTRACT

In this study we discuss atomic motion at the surface of a silicon single crystal. The theory which explains the reduction of intensity of LEED beams in terms of surface atomic motion is reviewed. We discuss silicon (111) surface reconstruction, and review surface models which have been offered to explain reconstruction.

We present the intensity-vs-voltage curve for the (00) beam of silicon (111) for both the (1×1) and (7×7) surfaces. We present data of the temperature dependence of the (00) beam intensity at various energies. Values of $\overline{u_\perp^2}$, the mean square displacement of surface atoms normal to the surface plane, are given at these energies, and discussed with reference to the intensity-vs-voltage data. Finally, we examine the effect of reconstruction upon the effective $\overline{u_\perp^2}$, measured at a Bragg reflection.

I. INTRODUCTION

A. Mean-Square Displacement of Surface Atoms

The subject of this study is the mean-square amplitude, $\overline{u_\perp^2}$, of the vibration of surface atoms in the silicon (111) crystal face in the direction normal to the surface. On a simple, intuitive level, surface atoms, which are bound to neighboring atoms in the bulk on one side but are not bound in the normal direction on the vacuum side, would be expected to vibrate with larger amplitudes than would atoms of the bulk. Viewing the bulk atoms of crystal lattice as bonded, in each of the three mutually perpendicular directions, by an effective force constant, the surface atomic layer would be expected to be more loosely bound with a reduced force constant. Furthermore, binding in the normal direction would be affected more than binding in the parallel direction.

Theoretical calculations of mean-square displacement of atoms have supported this intuitive idea, and have indicated an anisotropy between displacement in the directions normal and parallel to the surface. Clark, Herman and Wallis[1] have calculated $\overline{u_\parallel^2}$ and $\overline{u_\perp^2}$ of atoms in nickel crystals (fcc lattice) with free surfaces parallel to the (100), (110) and (111) planes, using a nearest-neighbor, force constant model. In all cases, both $\overline{u_\parallel^2}$ and $\overline{u_\perp^2}$ converge rapidly to the bulk values within five atomic layers. All cases show considerable anisotropy, with $\overline{u_\perp^2}/\overline{u_\parallel^2} = 1.54$ at the surface of the (111) face, for instance. This result is consistent with a qualitative notion that the creation of a free surface reduces forces affecting perpendicular motion more than forces affecting parallel motion.

Allen and DeWette[2,3] have performed theoretical calculations of $\overline{u_\perp^2}$ and $\overline{u_\parallel^2}$ for an fcc noble gas crystal, in which the atoms interact through a Lennard-Jones potential. Use of a potential rather than a force constant model is advantageous for several reasons. To begin with, calculation of changes in spacing between atomic layers parallel to the surface is possible. Allen and DeWette calculate interlayer spacings for static (non-vibrating) lattices and find rapid convergence to the bulk layer spacing. Calculated values of the increased spacing near the surface are then used to determine the changes in force constants near the surface. Thus, force constants corrected for the presence of a free surface are used in calculations of $\overline{u^2}$. As well, the asymmetry of the vibration of surface atoms in the normal direction can be taken into account. This asymmetry arises since the amplitude of motion is limited, in the bulk direction, by repulsion of neighbors, and in the outward direction, by attraction of the atoms of the crystal. Asymmetry of repulsive and attractive forces results in an outward shift of the mean atomic position. The degree of asymmetry, and hence the magnitude of the shift, increases with amplitude of vibration and is, therefore, strongly dependent upon temperature. For the (111) face, Allen and DeWette, give a value of $u^2_{\perp\,\text{surface}}/u^2_{\text{bulk}}$ which is smaller than that of Clark, Herman and Wallis.

B. LEED Measurements

Structural properties of an ordered crystal surface may be investigated by low energy electron diffraction (LEED). A collimated, monoenergetic beam of electrons is back-scattered by the crystal surface. Unlike X-rays, which penetrate the bulk, electrons in the range 0-500 eV

penetrate only several atomic layers. Electrons, with their relatively large scattering cross-section, are strongly back-scattered. Diffraction information can be obtained from the electrons that are scattered elastically. Because of the wave nature of electrons, constructive interference of the elastically back-scattered electrons results in beams which, when incident upon a fluorescent screen, produce a pattern. From this pattern, information concerning the ordered surface which produced it may be inferred.

If $\underset{\sim}{K}$ is the wave-vector of the primary electron beam and $\underset{\sim}{K}'$ is the wave-vector of the scattered beam, then the conditions for constructive interference may be written:

$$|\underset{\sim}{K}'| = |\underset{\sim}{K}| \tag{1}$$

$$\underset{\sim}{K}'_{\|} - \underset{\sim}{K}_{\|} \equiv \Delta\underset{\sim}{K}_{\|} = 2\pi\underset{\sim}{G} \tag{2}$$

where $\underset{\sim}{G}$ is a vector of the reciprocal lattice of the surface. In this study, the (00) beam intensity is measured for a range of energies and angles of incidence. For the (00) beam, which is at the specular angle with respect to the primary beam, $\Delta\underset{\sim}{K}_{\|} = 0$ and $|\Delta\underset{\sim}{K}_{\perp}| = 2|\underset{\sim}{K}|\cos\theta$, where θ is the angle of incidence, measured between $\underset{\sim}{K}$ and the surface normal. In the case of the (00) beam, $\Delta\underset{\sim}{K}$ is normal to the surface. Variation of the primary beam energy, measured in volts, changes $|\underset{\sim}{K}|$, through the relations:

$$\lambda = [150/V]^{\sim 1/2} \quad \text{and} \quad |\underset{\sim}{K}| = 2\pi/\lambda$$

where λ is measured in angstroms. V is the beam energy, and λ, the wavelength, is measured in angstroms.

The thermal dependence of the intensity of the (00) beam allows measurement of $\overline{u_{\perp}^2}_{surface}$. The reduction of intensity of LEED beams with increase in temperature is given by:

$$I = I_{rigid}\, e^{-2M}$$

where I_{rigid} is the intensity which would be produced by a non-vibrating lattice and M is a function of $\overline{u^2}$. For the (00) beam, $\Delta\underset{\sim}{K} = \Delta K_{\perp}$, which means that in the above equation, M depends on $\overline{u_{\perp}^2}$. For other beams, $\Delta\underset{\sim}{K}$ has components both parallel to and normal to the surface, so that the decrease in intensity with increased temperature would be related to an increase both in $\overline{u_{\perp}^2}$ and $\overline{u_{\parallel}^2}$. In that case, measurement of the factor M would show the anistropy of $\overline{u^2}$.

Derivation of the term e^{-2M} is given by James.[4] A brief outline of the derivation will be given here. If the atomic positions $\underset{\sim}{r}_i$ are altered, due to thermal motion, by random displacement vectors $\underset{\sim}{u}_i$, the expression for the scattered intensity at a point $\underset{\sim}{R}$ far from the crystal is:

$$I = \frac{|\Phi_o^2|}{R^2} \sum_n \sum_m e^{-i2\pi(\underset{\sim}{r}_n - \underset{\sim}{r}_m)\cdot\Delta\underset{\sim}{K}}\, e^{-i2\pi\overline{(\underset{\sim}{u}_n - \underset{\sim}{u}_m)\cdot\Delta\underset{\sim}{K}}}$$

Φ_o represents the amplitude of a scattered wave of a unit distance from the scattering point in the direction of $\Delta\underset{\sim}{K}$. Assuming atomic displacements obey a harmonic oscillator model,

$$e^{-iP_{n,m}} = e^{-\frac{1}{2}P_{n,m}^2},$$

where $P_{n,m} = 2\pi(\underset{\sim}{u}_n - \underset{\sim}{u}_m)\cdot\Delta\underset{\sim}{K}$. Then,

$$2\pi(\underset{\sim}{u}_n - \underset{\sim}{u}_m)\cdot\Delta\underset{\sim}{K} = \frac{4\pi\cos\theta}{\lambda}\,(u_{nK} - u_{mK})$$

where u_{jK} is the component of the displacement of the j^{th} atom in the direction of $\Delta\underset{\sim}{K}$. Assuming, for the moment, that atoms of the lattice vibrate independently, all possessing the same mean thermal energy,

$$\overline{u_{nK}u_{mK}} = 0$$

so that

$$\overline{(u_{nK} - u_{mK})^2} = \overline{u_{nK}^2} + \overline{u_{mK}^2} = \overline{2u_K^2} \quad .$$

If those assumptions hold, then if

$$M = 8\pi^2 u_K^2 (\cos^2\theta)/\lambda^2$$

the total scattered intensity becomes:

$$I = \frac{|\Phi_o|^2}{R^2} N(1 - e^{-2M}) + J_o e^{-2M} \quad .$$

The term in parenthesis increases with $\overline{u_K^2}$ and hence with temperature. It gives the contribution due to thermal diffuse scattering. The second decreases with increased $\overline{u_K^2}$, with J_o equal to the intensity scattered by the rigid non-vibrating lattice. If the diffuse background is subtracted from the intensity of a beam, the natural logarithm of the difference gives M, and hence $\overline{u_K^2}$.

James derives the factor M in another form, by summing over frequencies of the normal modes of the crystal.[5] For a cubic lattice with lattice parameter a and atomic mass m,

$$2M = \frac{16\pi^3}{3} |\Delta K|^2 \frac{\hbar}{m} \left(\frac{a}{2\pi}\right)^3 \sum_j \frac{1}{v_j^3} \int_0^{\omega_{mj}} \left[1/\left(e^{\hbar\omega/K_B T} - 1\right) + \frac{1}{2}\right] \omega d\omega$$

where the integration is over all frequencies of the normal vibrational modes of the crystal, and ω_{mj} is a maximum frequency. In the integrand, a factor of 1/2, which accounts for zero-point motion, is added to the average quantum number of a harmonic oscillator, given by the Planck distribution. The summation is over the three independent directions of vibration, and v_j is the velocity of a wave of type j. Assuming a mean value of the integral for different j, the above expression can be written:

$$2M = \frac{6h^2T}{mk\Theta_D^2}\left[\Phi(x) + \frac{x}{4}\right]\frac{\cos^2\theta}{\lambda^2}$$

where $x = \hbar\omega_m/kT$. The factor Θ_D is the effective Debye temperature, equal to $\hbar\omega_m/k$.

The expression in brackets is, for high temperatures or small x, approximately equal to 1. James gives values for the bracketed expression for $0 < x < 2.5$. For $0 < x < 1.5$, the value deviates from unity only by several percent. In this study, the approximate form of M will be used. Therefore, the temperature range over which intensity data may be taken without significant error is restricted. This consideration is discussed in Section II.

Equating the two expressions for M, and specifying the (00) beam gives, in the high temperature limit

$$\overline{u_K^2} = \overline{u_\perp^2} = \frac{3h^2T}{4\pi^2 mk_B\Theta_D^2}$$

A measurement of M for a particular λ will give a value of $u_\perp^2$ and hence a value of Θ_D^2.

However, an important reservation must be kept in mind. The above expressions for M assume the validity of the X-ray, or single-scattering case. In the case of scattered electrons, multiple scattering is important because of the larger scattering cross-section. Intensity due to electrons which have undergone two or more scattering events could not be expected to show the same thermal dependence as intensity due to electrons which have been scattered only once. The effects of multiple scattering will be discussed in Section III.

Since the electron beam does penetrate several atomic layers, the periodicity of atomic spacing results in enhanced intensity of the scattered beam when the wavelength of the primary beam obeys the relation

$$n\lambda = 2d\cos\theta \quad .$$

The experiments of this study used the (111) face of silicon so that $d = d_{111}$, the separation between equivalent atomic planes in the (111) direction. At such values of λ, determined by the θ-dependence of the energy, the intensity is due primarily to single scattering. At these energies, the thermal dependence could be expected to most nearly obey the derived relations for M.

Since the penetration depth of electrons increases with energy above about 10 eV, the measured u_1^2 should include larger contributions from the bulk at higher energies. Accordingly, the measured u_1^2 at Bragg energies should decrease (or equivalently, Θ_D should increase) as the energy of the primary beam increases.

C. Si(111) Surface Reconstruction

LEED studies have shown that many semiconductors have surface atomic arrangements which are different from the surface arrangement which would result simply from projection of the bulk.[6,7] In particular, clean Si(111) surfaces are characterized by atomic ordering of different types. There has been considerable interest in the (111) face of silicon. This may be because silicon cleaves along the (111) plane and because most silicon devices are fabricated with (111) oriented slices.[11]

In LEED studies, a change from one type of surface ordering to another produces a change in the observed LEED pattern. J. J. Lander[8] has reviewed early studies of atomic rearrangements on various metals and semiconductors, including silicon. The reciprocal lattice of a two-dimensional grating is conveniently viewed as consisting of parallel rods. The points of intersection between these rods and an Ewald sphere whose radius is equal to $|\underset{\sim}{K}_o|$ correspond to diffracted beams. If the surface unit cell vectors are both lengthened by a factor n (due to surface rearrangement), the separation of these rods in reciprocal space is decreased by the factor 1/n. Integer value multiples of unit cell vectors of the reconstructed surface in reference the substrate unit cell vectors are assumed using the (n×m) rotation. If the surface unit cell vector in one direction is lengthened and the other is not, spacing between rods will be reduced in the first direction and not in the second. Thus, the (n×1) surface thus does not produce a complete set of 1/n order spots.

In the case of silicon (111), surface structures depend both on the preparation and on the thermal history of the crystal. If a Si(111) surface is produced by cleavage in vacuum, a (2×1) surface results. After annealing at temperatures above 200°C, LEED indicates a transformation to a (1×1) structure. Annealing at higher temperatures (above 550°C) produces a (7×7) structure. These two surface transformations are both irreversible.[10] At still higher temperatures (865-890°C) a reversible transition to a (1×1) structure is seen.[11] This transition apparently involves not only loss of long-range order on the surface, but also a change in the separation between the first two atomic layers.

The (2×1) LEED pattern shows the appearance of 1/2-order beams, giving a pattern with 2-fold rotational symmetry.[12] These 1/2-order beams disappear as the (1×1) pattern with 6-fold symmetry appears. The 6-fold symmetry is maintained as the 1/7-order beams appear.

In this work, a clean surface was obtained by ion bombardment, and not by cleavage, so that the (2×1) structure was not seen. Annealing produced (1×1) and (7×7) structures. Bombardment at room temperature then removed the (7×7) surface each time the crystal was cleaned.

The idea that the (2×1) and (7×7) structures may be impurity stabilized has now been laid to rest. Auger studies[13,14] have established the cleanliness of a surface with (7×7) structure. Cleavage of silicon at 850°C produces a (7×7) pattern within 9 sec, a time too short for diffusion of impurities surface, or adsorption of gas impurities, to be important. Surface reconstruction is an intrinsic property of clean silicon.[15]

Models have been proposed to account for silicon surface reconstruction. Most notable are the models of Haneman[16-18] and of Lander and Morison.[19-21] Both give mechanisms to explain the changes in the surface unit vector lengths with reconstruction. Figure 1 is a photograph showing the unreconstructed Si(111) surface (diamond lattice).[22]

Lander and Morrison offer, for the (2×1) and (7×7) structures, models which feature double bonds among surface atoms. To explain the (2×1) structure they suggest that surface atoms of alternating vertical rows are displaced laterally and doubly bonded to atoms of rows which were not displaced, while atoms of the second layer also form paired rows. Their suggested (7×7) structure involves, first, the removal of approximately 3/4 of the surface atoms. Next, the surface atoms are doubly bonded to atoms of the second layer to form warped benzene rings in "phenalene" arrangements.

Haneman's model involves a modification of the sp^3 tetrahedral bonding scheme to raise and lower surface atoms in the direction normal to the surface. Each atom of the unreconstructed surface is bonded to three atoms of the second layer, with one "dangling bond". If the dangling bond is allowed to become more p-type, the remaining three become more sp^2-type, and hence more trigonal, so that the atom in question is lowered. Resultant lateral forces are relieved if alternate surface atoms are raised. Assuming a Morse potential for the interatomic interactions, Haneman and Taloni[18] have computed the surface energy for the "buckled" surface. finding it to be lower than the energy of the "normal", unbuckled surface.

According to a more recent view of silicon surface reconstruction, the Haneman model adequately describes the structure of the (2×1) surface and a qualitatively different model is required to describe the (7×7) structure. Phillips and Rowe[12] display ultraviolet photoemission spectroscopy (UPS) data to support their contention that the surface-vacancy model of Lander and Morrison gives an accurate picture of the (7×7) surface. For the (2×1) surface, they identify the contribution to the UPS spectrum due to the "dangling bond" surface state. For the (7×7) surface, they identify the contribution due to the conjugated double bonds of the phenalene-like rings of the Lander model.

No model similar to Haneman's has been offered for the (7×7) surface. The (7×7) structure occurs only at elevated temperatures, and while the Haneman model seems plausible as a description of surface relaxation following cleavage, it is unclear why a similar (7×7) mechanism would require increased thermal energy. Of course, a Haneman model for the (7×7) can be imagined: the seventh atom along every seventh row may be raised relative to the unrelaxed surface. However, it appears unlikely that this mechanism would be activated. The Lander-Morrison model, however, appears plausible for the (7×7) structure because it involves the migration of surface defects. Since surface migration of silicon atoms is very slow below about 600°C,[21] it is reasonable that the vacancy-model (7×7), which is more stable than the (1×1) even at lower temperatures, would form only at elevated temperatures.

II. EXPERIMENTAL

A. Apparatus and Crystal Preparation

The LEED experiments of this study were performed in a stainless steel chamber with copper sealing gaskets at mating flanges. Pressure between 8×10^{-10} and 2×10^{-9} torr was maintained in the chamber by an ion pump. A titanium sublimator provided pumping while ion bombardment of the crystal was in progress.

The silicon crystal used was p-type of 2.5×10^{3} Ω-cm resistivity. The crystal was oriented roughly in the (111) direction by Laue X-ray diffraction before cutting. A wafer was then cut with a diamond-tipped blade. After cutting, the wafer was oriented to within better than 0.5° of the (111) face. It was then mechanically polished.

A heater was constructed of high density, high purity alumina, and fitted with a filament of tantalum wire of 0.15 in. diameter. The filament rested in the crystal holder behind the silicon sample, which was heated radiatively. The filament was wound in such a way that magnetic fields created by the heater current would be approximately self-cancelling. In this way, high heater current would not interfere to any appreciable degree with the diffraction pattern produced by low energy electrons scattered by the crystal. A current of 9 amperes was required to reach temperatures between 800°C and 850°C at the surface of the crystal. Three molybdenum clamps held the crystal in place.

The crystal was cleaned in the apparatus by ion bombardment and annealing. Argon ions of 2.0 keV energy were used, at an argon pressure of 5×10^{-5} torr. Usually, alternate bombardment and annealing treatments were required to remove all carbon and oxygen, the principal surface

contaminants. The crystal was annealed at 800°C-900°C, except when a 1×1 (unreconstructed) surface was required. In that case, the crystal was annealed at 350°C-400°C.

Surface impurity levels were monitored by Auger electron spectroscopy. Of the two principal impurities, carbon was the more difficult to remove by bombardment. Measurement of silicon and carbon peaks, and use of the known 2/1 ratio between silicon (91 eV) and carbon (272 eV) Auger cross sections showed that in the worst cases, bombardment for about 20 min left approximately 0.002 monolayer of carbon. Annealing and continued bombardment removed carbon altogether. Figure 2 is an Auger spectrum for a surface which is acceptably clean, showing the silicon peaks in the 0-120 eV range. The peaks at 44 and 91 eV are due to Auger transitions. The peaks at 74 and 57 eV are due to first- and second-order bulk plasmon losses associated with the 91 eV peak. The peak at 107 eV has not been assigned.[15,23]

Anneals above 800°C or at 300-400°C produced (7×7) or (1×1) patterns, respectively. The (7×7) features were visible after anneals to 700°C. Erbudak and Fischer[10] remark that this (7×7) appearance temperature decreases with decreased background pressure, suggesting that the reactivity of the (1×1) surface with contaminant gases inhibits the formation of the (7×7). In this work the pressure dependence of the appearance temperature was not studied. Figure 3 is a photograph of a (7×7) diffraction pattern.

B. Measurement of LEED Intensity and Surface Temperature

The crystal was rotated to bring the (00) beam into view. The intensity of the spot was then measured by a model 2000 telephotometer. In most cases, the fiber aperture with an acceptance angle of 20 min was used. The output of the telephotometer passed through a low-pass RC filter, which reduced noise, and then into the vertical axis input of a chart recorder.

It was found that, possibly due to thermal stress in the crystal holder, the (00) spot moved, on occasion, by 10-15 min. For this reason, once intensity measurements had commenced, the angular position of the manipulator was no longer taken as a reliable indicator of angle. Rather, the telephotometer optical head was locked into place on its tripod. In this way, since the incident beam direction and telephotometer position were fixed, the angle of incidence, once measured, remained fixed.

The background measurements were taken 3° from the (00) beam. The manipulator, not the telephotometer, was moved to the background position. In order to reposition the manipulator, the (00) beam, at its most intense energy peak (96 eV) was moved to center the (00) spot at the cross hair of the telephotometer. The beam energy was then accurately returned to its former value by means of a six-digit voltmeter.

There are three widely used techniques for measurement of Debye Waller factors: (1) transient; (2) steady-state; and (3) point-by-point methods. Methods (2) and (3) are described by Somorjai and Lyon[24] and by Tabor, Wilson and Bastow,[25] respectively. Both (2) and (3) involve measurement of intensity at fixed temperature. In method (2), an intensity vs voltage curve is obtained over a range of several hundred eV at a fixed temperature. In method (3), the intensity of a particular peak is

maximized, at fixed temperature, by adjustment of the electron beam voltage. These techniques are often necessary when bulk expansion is important. Lattice expansion would have the effect of reducing the spacing among diffracted beams, thus changing the positions of all spots other than the (00) spot. In this work, the (00) beam is used.

As well, lattice expansion, if significant, would shift Bragg peaks to lower energies through the relation $n\lambda = 2d\cos\theta$. For silicon, however, with its low coefficient of thermal expansion ($1.0\text{-}4.5\times10^{-6}$/°C in the temperature range 200-1000°K[26]), this effect is not noticeable. Figure 4 shows intensity vs voltage curves for the silicon (111) Bragg peak at 137 eV for various temperatures between 200 and 530°C. Increased lattice spacing might be expected to produce a peak shift to lower energies with increased temperature, through the relation $n\lambda = 2d_{111}\cos\theta$, where $\lambda \propto E^{-1/2}$. However, no measurable peak shift larger than 0.5 eV in this temperature range is observed.

Accordingly, method (1) was used in this study. The crystal was heated to about 550°C, and the heater current was then turned off. The intensity of the (00) beam was measured as a function of thermocouple voltage as the crystal cooled to about 200°C. The crystal was then rotated by 3°, and a measurement of background intensity was taken over the same temperature range. Figure 5 shows a plot of intensity vs thermocouple voltage for the (00) beam and background, at 96 eV.

Of the five values of Θ_D in this study, four (57, 96, 117 and I36 eV) lie between 400°K and 500°K. Therefore, if data is accepted over a range of 350-550°C, then for each of these four measurements, the value of Θ_D/T ranges between about 0.53 and 0.7. In this range, the function

$\{\Phi(x) + x/4\}$, $x = \Theta_D/T$, discussed in Chapter I, varies by less than 1%. The value of Θ_D at 256 eV is approximately 700°K. Here, data in the higher temperature range, 400-500°C, is accepted. The function then varies by approximately 1%. And so, the approximate (high temperature) form of the Debye-Waller factor holds to within 1%.

There were two serious problems in the measurement of the surface temperature. First, several metals commonly used in thermocouples form, with silicon, alloys whose eutectic points lie below 1000°C, within the temperature region of interest in this study. A chromel-alumel thermocouple melted above about 750°C. (The aluminum-silicon eutectic is at 577°C.[27]) A platinum-rhodium thermocouple was also unsatisfactory. (The platinum-silicon eutectic is at 980°C, and platinum silicide forms readily on atomically clean silicon by a solid-solid reaction above 300°C.[28]) This problem was solved by use of a tungsten-5% rhenium/tungsten-26% rhenium thermocouple. Tungsten does not form a liquid phase with silicon below 1400°C.[29]

Second, since the sensing element of the thermocouple cannot be reliably spot-welded to silicon, accurate measurement of the surface temperature of silicon is notoriously difficult.[30] The thermocouple voltage indicated a surface temperature about 100°C below the temperature measured with an accurately calibrated optical pyrometer in the 750-900°C range.

This problem was solved by calibration of the thermocouple with an infrascope. The infrascope was first calibrated against a source which was assumed to approximate a black body radiator. A hole of about 0.5 cm in diameter and about 3 cm in depth was drilled

in a graphite block which was placed within an oven. Through a hole in the oven door the temperature of this "black body" was measured by a thermometer and by the infrascope. The infrascope was thus calibrated, with the emissivity control set at 1.0.

Next, the crystal temperature was measured by the optical pyrometer at about 800°C, and the emissivity control of the infrascope was adjusted to give the same reading. This adjustment gave a value of 0.55 for the measured effective emissivity of the silicon crystal viewed through a glass port. Finally, the infrascope, with this emissivity value, was used to calibrate the thermocouple.

III. RESULTS AND DISCUSSION

A. Intensity vs Voltage Curves

Figure 6 shows the (00) beam intensity vs voltage curves for the (1×1) and (7×7) surfaces in the range 50-150 eV, taken at an incident angle of 4°. The azimuthal angle was 30°. Peaks appear at 47-57, 96 117 and 137 eV. In this range, reconstruction to give the (7×7) surface alters the relative magnitudes of the peaks. The major difference between the two curves is the increased intensity of the peak at 137 eV relative to the intensity of the peaks at 47-57 eV with reconstruction. The voltages are the "external" values, not corrected for contact potential differences or for inner potential. In Fig. 7, the intensity curve for the (7×7) surface is shown in the 200-350 eV range. Bragg peaks are at 256 and 325 eV.

Theeten, Domange and Bonnerot have studied the intensity-voltage characteristics of the (7×7) surface.[32] Their results are similar to the results obtained here, with the following differences. First, the peak positions given here are shifted to higher energies, by an approximately constant factor, relative to the peak positions given by Theeten, et al. Second, they do not report a peak corresponding to the one which appears at 117 eV. Third, they report that reconstruction to give the (7×7) surface decreases the intensity of the peak at 137 eV relative to the intensity of the peaks at 47-57 eV.

The first discrepancy may be due to voltage calibration. The second and third are probably due to differences in azimuthal angle, which Theeten, et al. do not report. Here, the designation of azimuthal angle will follow the convention established by Jona.[31] The azimuthal

angle, ϕ, is 30° at normal incidence. Using Jona's notation, the (10), $(\bar{1}1)$ and $(0\bar{1})$ beams show a strong intensity maximum at 84 eV and the (01), $(\bar{1}0)$ and $(1\bar{1})$ beams almost vanish. At 110 eV, the second set of beams shows a strong maximum and the first set almost vanishes. These maxima are marked and can easily be seen with the unaided eye. No attempt was made to make quantitative measurements of intensity on beams other than the (00).

Theeten, et al. give, as an approximation to the Bragg formula in cases where the inner potential, V_o, is small relative to $V_{external}$, and where θ is small:

$$V_{ext} \cos^2\theta_{ext} = \text{constant}$$

When the θ-dependent behavior of the peaks at 137 and 256 eV was examined, this condition held to within about 2% over a θ-range of about 10°.

Further, using the value 3.9Å[11] for d_{111}, the spacing between equivalent (111) planes of silicon, the peaks at 137, 256 and 325 eV are designated as Bragg peaks of respective orders 6, 8 and 9. Theeten, et al. give 126, 237 and 296 eV as the positions of these Bragg peaks.

Figure 8 shows the intensity of the (00)-beam from the Si(111)-(7×7) surface at various angles of incidence in the range between 90 and 140 eV; and Fig. 9 shows a similar plot for the 110-130 eV range. Here, an angular range of only 4° is shown for both cases. In agreement with Theeten, et al. the 96 eV peak shifts very slowly (a shift of approximately 1 eV in an angular range of 6°) as compared to the peak at 137 eV. The 96 eV peak is expected to contain a contribution from n = 5 Bragg

scattering. In the angular range given there is no discernible shift in the peak at 117 eV.

The intensity at 57 eV is expected to include a contribution from n = 4 Bragg scattering. However, the difficulty of resolving the peaks at 47-57 eV made analysis of the angular dependence of the 57 eV peak difficult. This group of peaks appears to be dominated by two peaks separated by several eV (Fig. 6). The angular dependence of these peaks is uncertain.

B. Debye -Waller Measurements

Figure 10 gives the effective Debye temperatures measured in this study, calculated from logarithmic plots of intensity vs temperature displayed in Fig. 11. In Fig. 10 the values of θ_D reported by Theeten, et al. are included for comparison. In both studies data is taken for the (7×7) surface.

In computation of the Θ_D values corrected energies were used. V, the beam energy given by the LEED electrometer gives the potential between the Fermi levels of the cathode and the crystal. Thus, E, the free-electron energy, is given by:

$$E = V - V_c$$

where V_c is the differences between the crystal and cathode work functions ($V_c = \Phi_{crystal} - \Phi_{cathode}$).[9] For a tungsten cathode and silicon crystal, V_c is less than 1 eV, and can be ignored.

As an electron enters the crystal, it is accelerated in the direction normal to the surface. Its energy is increased by an inner potential, V_o, V_o = 10 eV for silicon.[11] If θ is the uncorrected angle of incidence, θ_c, the corrected angle is given by:

$$\sin\theta_c = \frac{E^{1/2}}{(E + V_o)^{1/2}} \sin\theta$$

In this study, θ is small enough so the angle correction is negligible for Debye-Waller calculations.

The values of Θ_D for the peaks at 96, 137 and 256 eV show similar variations in the two sets of data. Between 325 and 137 eV, the measured Θ_D decreases, as expected. Θ_D then rises for 117 and 96 eV, and falls for 56 eV. Discussion of measured Θ_D values at these energies clearly calls for consideration of effects which go beyond beam penetration as a function of energy. Here, secondary (multiple) scattering will be considered.

The values of Θ_D at 57, 96 and 137 eV are larger than Θ_D for 137 eV, where Bragg scattering apparently dominates. This effect may be due to a large secondary scattering contribution. Tabor, Wilson and Bastow,[25] have discussed possible effects of multiple scattering on the effective Θ_D. Tabor et al. consider the (00) beam. If scattering into the (00) beam is accomplished via two reciprocal lattice vectors, $\underset{\sim}{G}_1$ and $\underset{\sim}{G}_2$, then the factor 2M can be written:

$$2M_{dd} = 2C\left[\frac{|\underset{\sim}{G}_1|^2}{\Theta_1^2} + \frac{\underset{\sim}{G}_1 \cdot \underset{\sim}{G}_2}{\Theta_1\Theta_2} + \frac{|\underset{\sim}{G}_2|^2}{\Theta_2^2}\right]$$

where Θ_1 and Θ_2 are the Debye temperatures associated with the G_1 and G_2 directions and C is a constant. In the case considered by Tabor, et al., $\underset{\sim}{G}_1 \perp \underset{\sim}{G}_2$. If a kinematic (single) scattering event is considered,

$$2M_k = 2C\,\frac{|\underset{\sim}{G}_3|^2}{\Theta_3^2}$$

Assuming $\underset{\sim}{G}_1 \approx \underset{\sim}{G}_3$, then $\Theta_1 \approx \Theta_3$. If $\Theta_1 = \alpha\Theta_B'$ and $\Theta_2 = \beta\Theta_B$ where $\alpha, \beta < 1$ and Θ_B is the bulk value,

$$2M_{dd} = 2M_k + 2C \frac{|\underset{\sim}{G}_2|^2}{\Theta_B^2} \left(\frac{1}{\beta^2} - \frac{1}{\alpha^2}\right)$$

so that $2M_{dd}$ may be either larger or smaller than $2M_k$. Tabor et al. consider the special case in which $G_1 \perp G_2$. If this is not the case, the cross term must be added. If the cross term is small, the relation magnitudes of α and β will still determine the relative magnitudes of M_k and M_{dd}.

In the case of 57 and 96 eV, the measured Θ_D is larger, or, the measured 2M is smaller than expected assuming single scattering. This would result from $\alpha < \beta$ in the above equation, so that $\Theta_1 < \Theta_2$ and $\overline{u_1^2} > \overline{u_2^2}$. In this way, the values of Θ_D at 57, 96 and 137 eV may be due to a contribution from secondary scattering. Discussion in further detail would require knowledge of the particular reciprocal lattice vectors involved.

C. Effects of Reconstruction on Θ_D

The value Θ_D at 137 eV was measured for the (1×1) and (7×7) surfaces. The measurements were taken at a lower temperature range (460 to 250°C) to prevent the (1×1) surface from reconstructing while it was under study. Data was first taken for the (1×1) surface. The crystal was then annealed at 800-900°C for about 5 min, and the measurement repeated. As in other measurements, the telephotometer was not moved throughout the experiment, assuring that measurements for the (1×1) and (7×7) were taken at the same incidence angle.

The 137 eV peak was chosen for this study for two reasons. First, it does not exhibit the sort of anomalous behavior which the 57, 96 and 117 eV peaks exhibit. Results of both θ-dependence study and Debye temperature study, discussed earlier, support the claim that the peak at 137 eV is due primarily to kinematic scattering. Since secondary scattering effects can then be ignored, and it can be assumed that the measured Θ_D is associated with $\overline{u_\perp^2}$, and has no significant contribution from $u_\parallel^2$. Thus, the physical interpretation of the result is clearer. Second, the 137 eV peak gives a value of Θ_D sufficiently different from the bulk value so that surface reconstruction may be expected to produce a measurable effect. If a higher energy were used, the contribution from surface scattering would be smaller, and a change in the scattering by the surface layer would give a smaller change in the measured Θ_D.

The results are given in Fig. 12. Logarithmic plots of intensity vs temperature are shown for unreconstructed (1×1) and reconstructed (7×7) surfaces. Two sets of data are shown for each surface. The plots indicate that reconstruction decreases the effective Θ_D. For each of the four sets of data, the linear least-squares fit was computed. For each surface, (1×1) and (7×7), the average of the two slopes was then computed. The slope is greater by a factor of 1.07 (or, greater by 7%) for the (7×7) surface, indicating that according to the data presented, $u_\perp^2$ is larger by 7% for the (7×7) surface. The effective Θ_D, equal to 410°K for the (7×7) surface, is larger by approximately 3.5% for the (1×1) surface.

It is presumed that the (7×7) surface which gave the data shown here was "completely" reconstructed. In earlier work it was noted that

short anneals at 800-900° produced a sharp (7×7), and that annealing for longer times did not improve the apparent quality of the surface, as indicated by LEED.

LEED observations have suggested that reconstruction occurs over a temperature range.[10] Over this range, the quality of the (7×7) pattern improves with continued annealing. Presumably, the increase in the intensity of the (7×7) features is due to growth of the (7×7) ordered domain, or to improvement of surface ordering within an ordered domain, or to both of these processes. Improvement of the pattern presumably stops when both processes have stopped. At that time, a domain size equal to the coherence width of the beam has been achieved, and surface rearrangement within the domain has ceased. If the (7×7) domain were smaller than the coherence width of the beam, or if the surface within the domain were not fully reconstructed, a value of Θ_D intermediate between the values reported here for the (1×1) or (7×7) surfaces would be obtained.

The measured increase in $\overline{u_\perp^2}$ with reconstruction must be considered in connection with the model of surface reconstruction put forward by Lander and Morrison and later discussed by Rowe and Phillips. Two important features of this model would strongly affect surface atomic motion. First, sp^2 hybridization at the surface allows π-bonding among surface atoms. These double bonds would increase atomic binding, predominantly in the direction parallel to the surface. Binding in the normal direction would also be increased, though less dramatically. Hence, surface double bonding would tend to increase Θ_D, or decrease $\overline{u_\perp^2}$.

The second feature of this model is a large number of surface vacancies. The effect of vacancies would appose the effect of π-bonding upon the random displacements of surface atoms. The absence of surface atoms would tend to weaken forces giverning atomic motion in the directions both parallel and normal to the crystal surfaces.

ACKNOWLEDGEMENT

This work was done under the auspices of the U. S. Atomic Energy Commission through the Inorganic Materials Research Division, Lawrence Berkeley Laboratory.

REFERENCES

1. B. C. Clark, R. Herman and R. F. Wallis, Phys. Rev. 139, 860 (1965).
2. R. E. Allen and F. W. DeWette, Phys. Rev. 179, 873 (1969).
3. R. E. Allen and F. W. DeWette, Phys. Rev. 188, 1320 (1969).
4. R. W. James, Optical Principles of the Diffraction of X-Rays (Bell, London, 1962), Chapter 1.
5. Ibid., Chapter 5.
6. R. E. Schlier and H. E. Farnsworth, J. Chem. Phys. 30, 917 (1959).
7. D. Haneman, J. Chem. Phys. Solids 14, 162 (1960).
8. J. J. Lander, Progress in Solid State Chemistry 2, 26 (1965).
9. P. J. Estrup and E. G. McRae, Surf. Sci. 25, 1 (1971).
10. M. Erbudale and T. E. Fischer, Phys. Rev. Lett. 29, 732 (1972).
11. W. Monch, Adv. in Solid State Physics, XIII, 241 (1973).
12. J. E. Rowe and J. C. Phillips, Phys. Rev. Lett. 32, 1315 (1974).
13. D. Taylor, Surf. Sci. 15, 169 (1969).
14. T. J. Grant and T. W. Haas, Appl. Phys. Lett. 15, 140 (1969).
15. J. W. T. Ridgeway and D. Haneman, Appl. Phys. Lett. 14, 265 (1969).
16. W. J. T. Ridgeway and D. Haneman, Appl. Phys. Lett. 14, 269 (1969).
17. D. Haneman, Phys. Rev. 121, 1093 (1961).
18. A. Taloni and D. Haneman, Surf. Sci. 10, 215 (1968).
19. J. J. Lander and J. Morrison, J. Appl. Phys. 34, 1043 (1962).
20. J. J. Lander and J. Morrison, J. Chem. Phys. 37, 729 (1962).
21. J. J. Lander, G. W. Gobeli and J. Morrison, J. Appl. Phys. 34, 2298 (1963).
22. J. F. Nicholas, An Atlas of Models of Crystal Surfaces (Gordon and Breach, 1965).

23. T. J. Grant and T. W. Haas, Surf. Sci. 23, 347 (1970).

24. H. B. Lyon and G. A. Somorjai, J. Chem. Phys. 44, 3707 (1966).

25. D. Tabor, J. M. Wilson and T. J. Baston, Surf. Sci. 26, 471 (1971).

26. R. A. Evans, et al., Integrated Silicon Device Technology (Research Triangle Institute, Durham, N. C., 1964), Vol. V, p. 21.

27. R. Hultgren, et al., Selected Values of the Thermodynamic Properties of Binary Alloys (American Society for Metals, 1973), p. 212.

28. B. Schwartz, Ohmic Contacts to Semiconductors (University Microfilms, 1968), p. 166.

29. Ibid, p. 235.

30. F. Jona and H. R. Wendt, J. Appl. Phys. 37, 3637 (1966).

31. F. Jona, I. B. M. J. Res. Develop. 14, 444 (1970).

32. J. B. Theeten, J. L. Domange and J. Bonnerot, Sol. Stat. Comm. 8, 643 (1970).

33. E. G. McRae and P. J. Jennings, Surf. Sci. 15, 345 (1969).

34. E. G. McRae, Surf. Sci. 25, 491 (1971).

35. D. S. Boudreaux and V. Heine, Surf. Sci. 8, 426 (1967).

FIGURE CAPTIONS

Fig. 1. (111) surface of diamond lattice.

Fig. 2. Auger spectrum from clean silicon.

Fig. 3. LEED pattern of silicon (111)-(7×7) surface.

Fig. 4. 137 eV peak at various temperatures.

Fig. 5. Output of telephotometer, for (00) beam and background.

Fig. 6. Intensity vs voltage, (1×1) and (7×7) surfaces, 50-150 eV.

Fig. 7. Intensity vs voltage, (7×7) surface, 200-350 eV.

Fig. 8. Intensity vs voltage, 90-140 eV, for various angles of incidence.

Fig. 9. Intensity vs voltage, 110-130 eV, for various angles of incidence.

Fig. 10. Values for Θ_D and $\overline{u_\perp^2}^{1/2}$

Fig. 11. Plots of $\mathrm{Ln}(I - I_B)$ vs temperature, for various energies.

Fig. 12. Plots of $\mathrm{Ln}(I - I_B)$ vs temperature, at 137 eV, for (1×1) and (7×7) surfaces.

Diamond (111) $0 \leq \delta < \frac{1}{4}$

a_1 undefined; $\beta_1 = 0°$

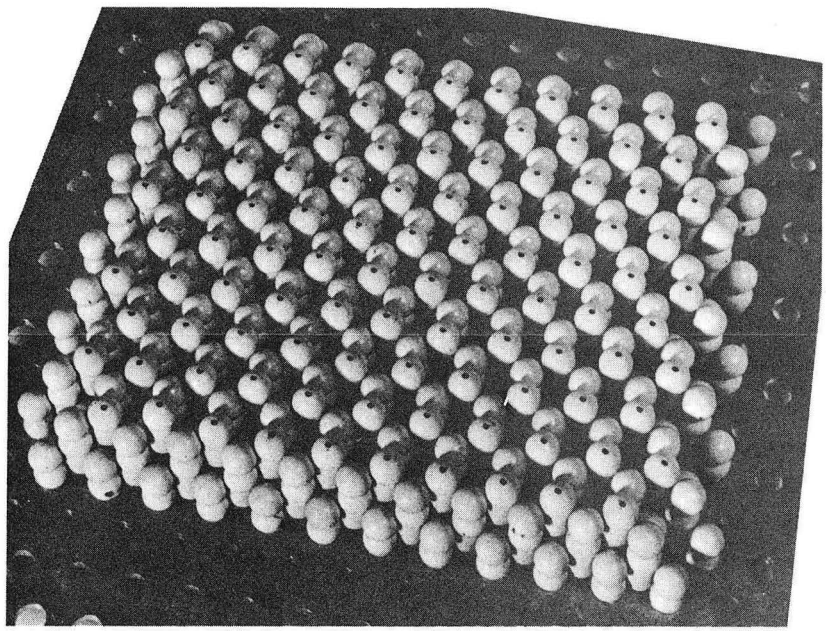

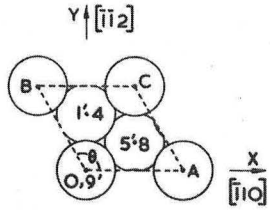

XBB 7412-8560

Fig. 1

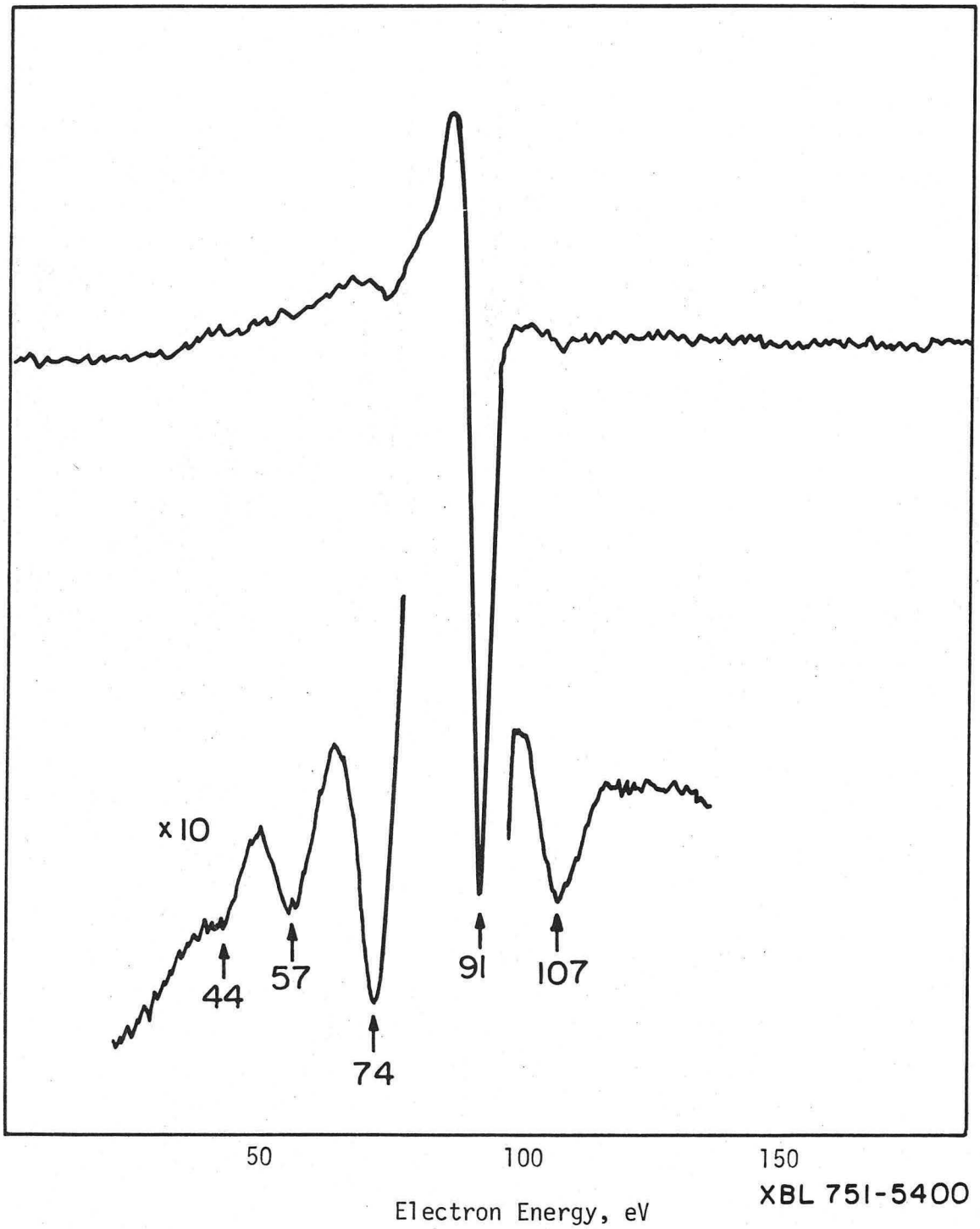

Fig. 2

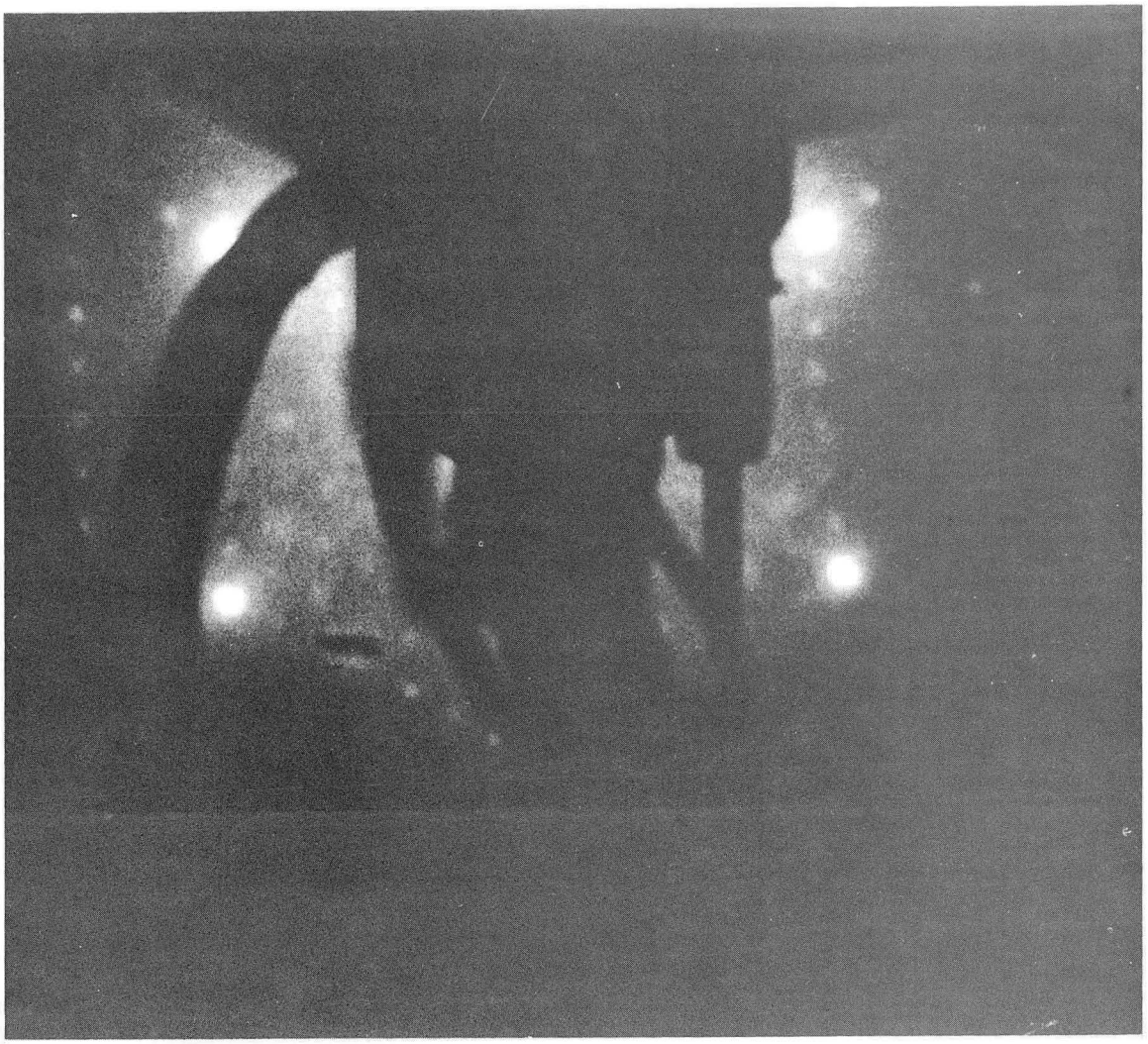

XBB 7412-8741

Fig. 3

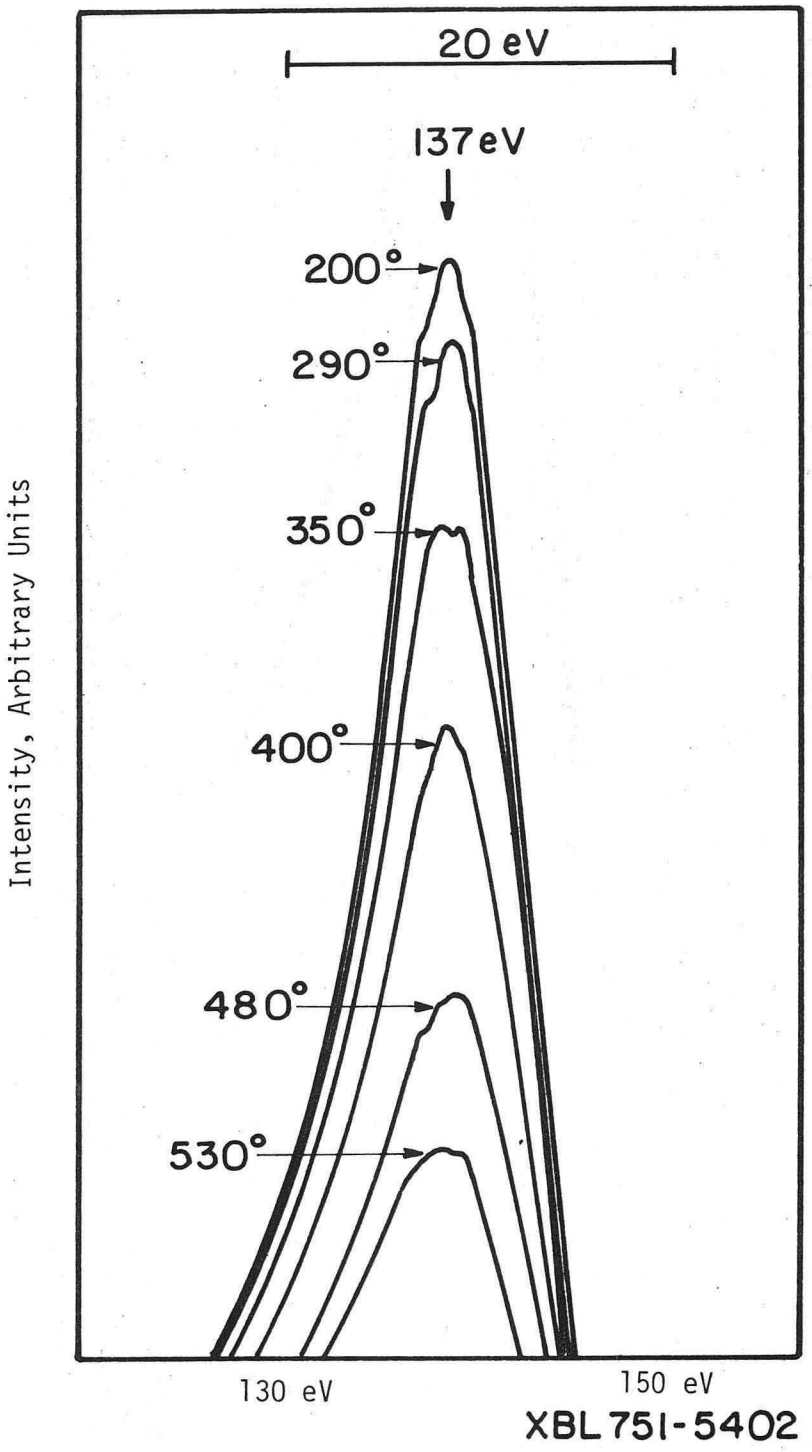
20 eV
137eV
200°
290°
350°
400°
480°
530°
130 eV
150 eV
XBL751-5402
Intensity, Arbitrary Units
Electron Energy

Fig. 4

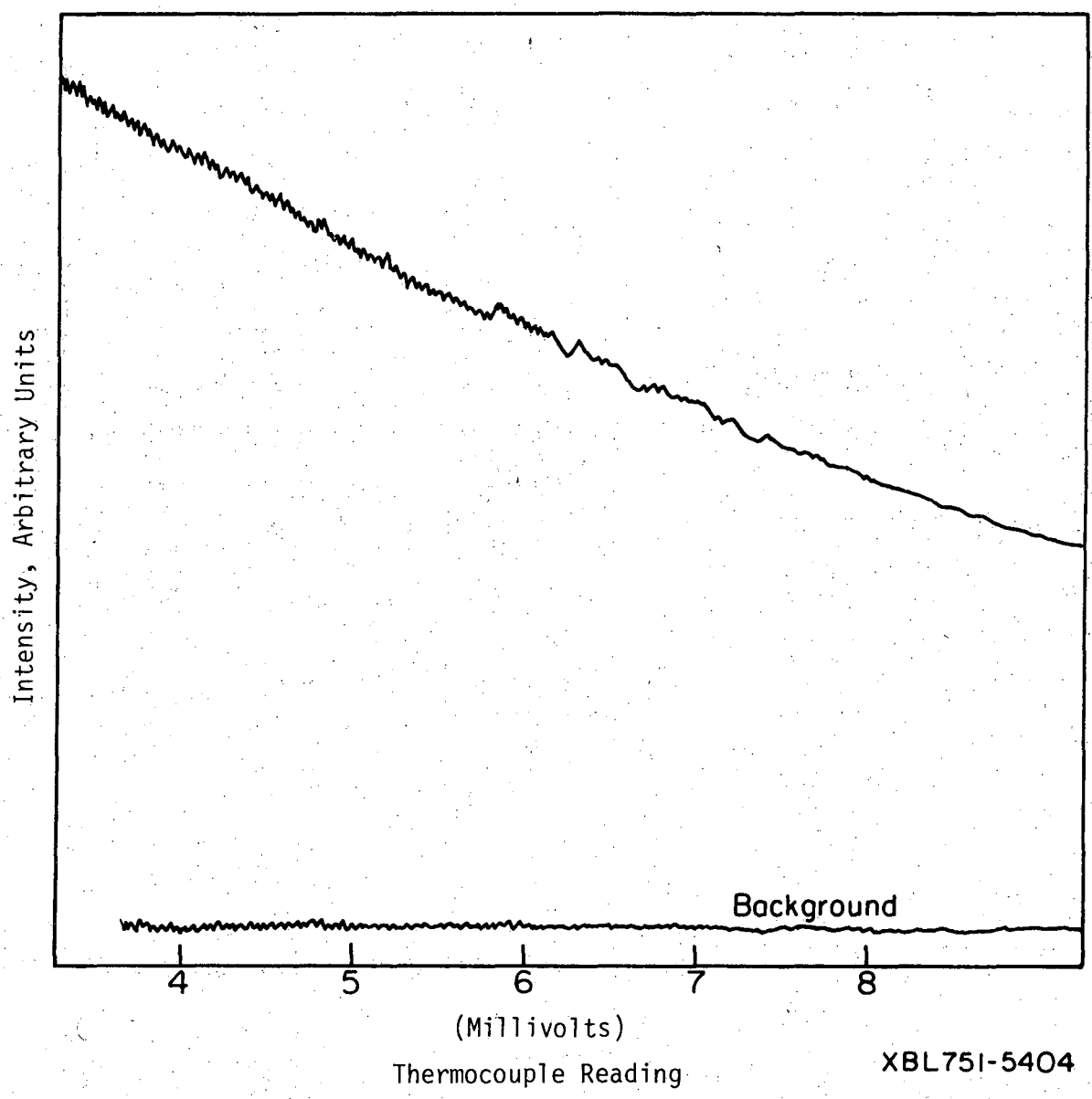

Fig. 5

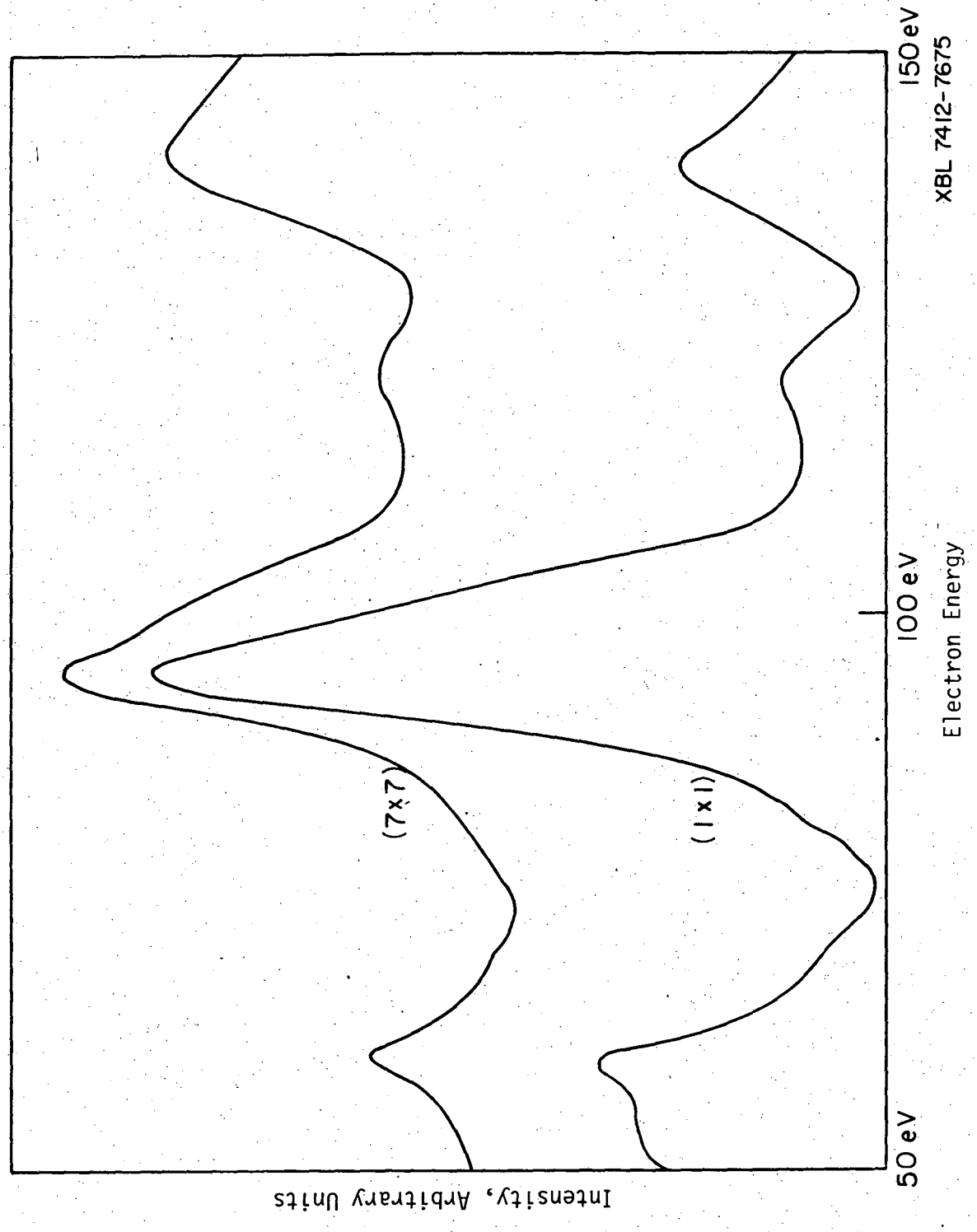
Intensity, Arbitrary Units
50 eV
100 eV
150 eV
Electron Energy
(7x7)
(1x1)
XBL 7412-7675

Fig. 6

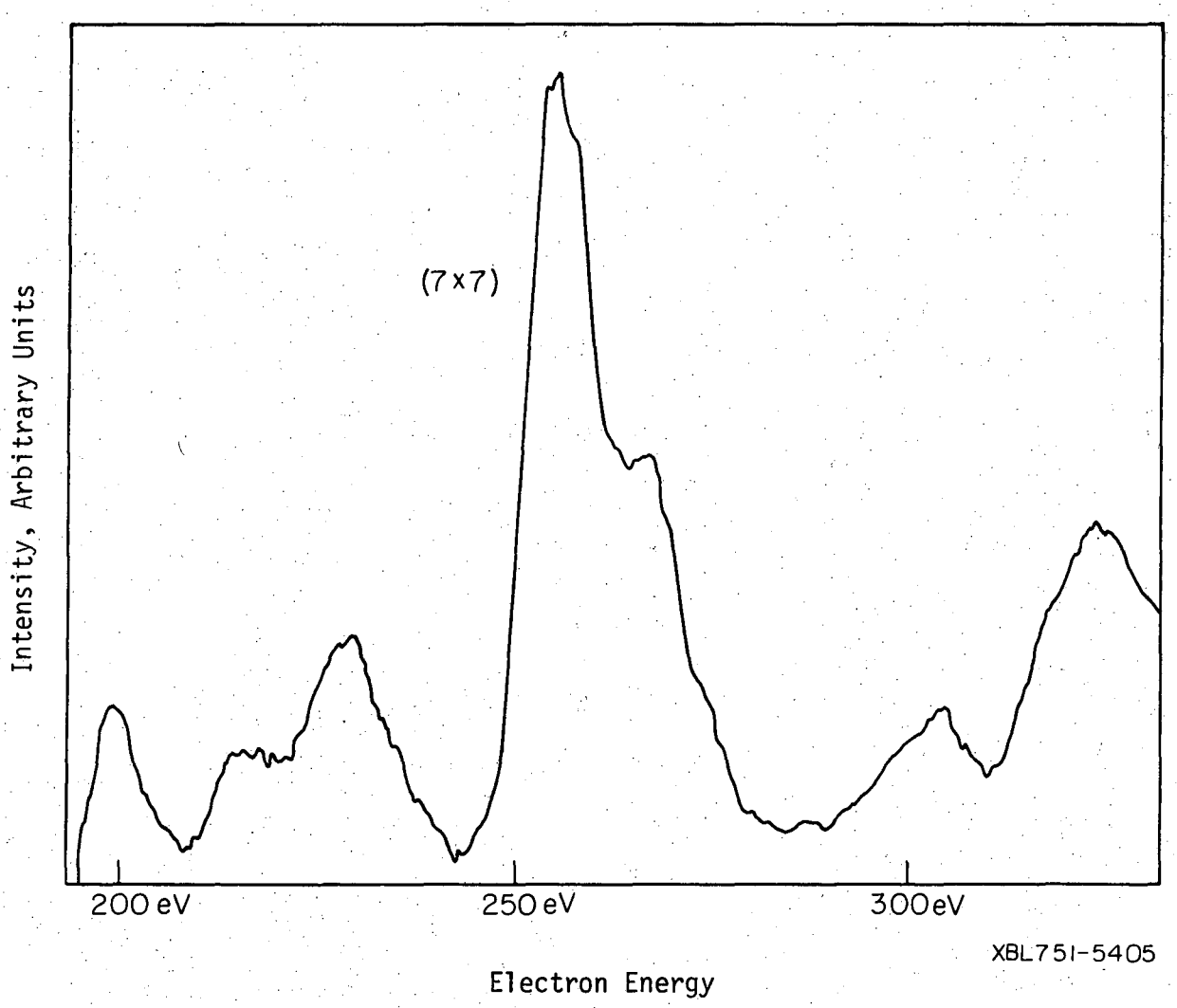

Fig. 7

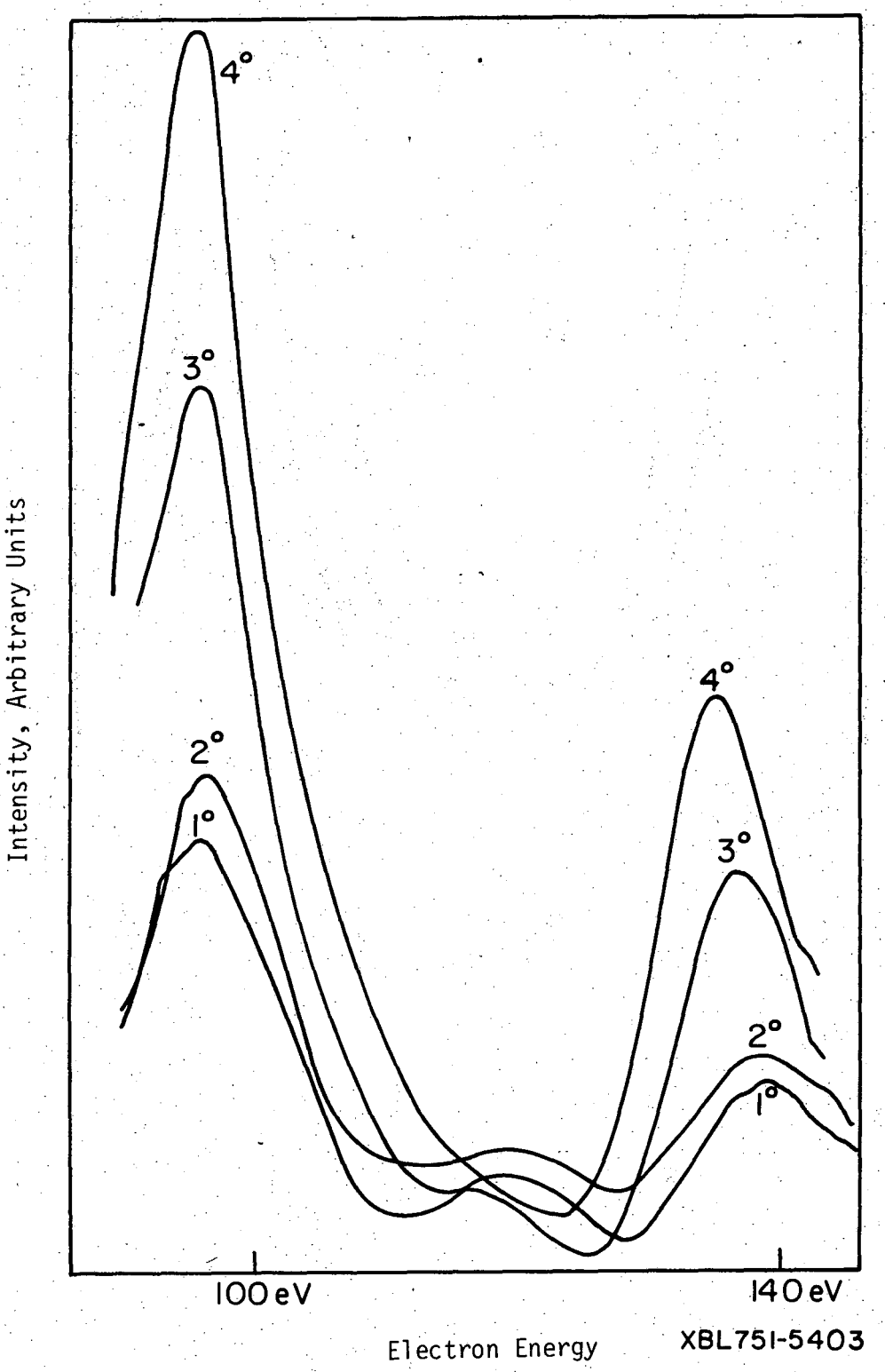
4°
3°
2°
1°
4°
3°
2°
1°
100 eV
140 eV
Intensity, Arbitrary Units
Electron Energy
XBL751-5403

Fig. 8

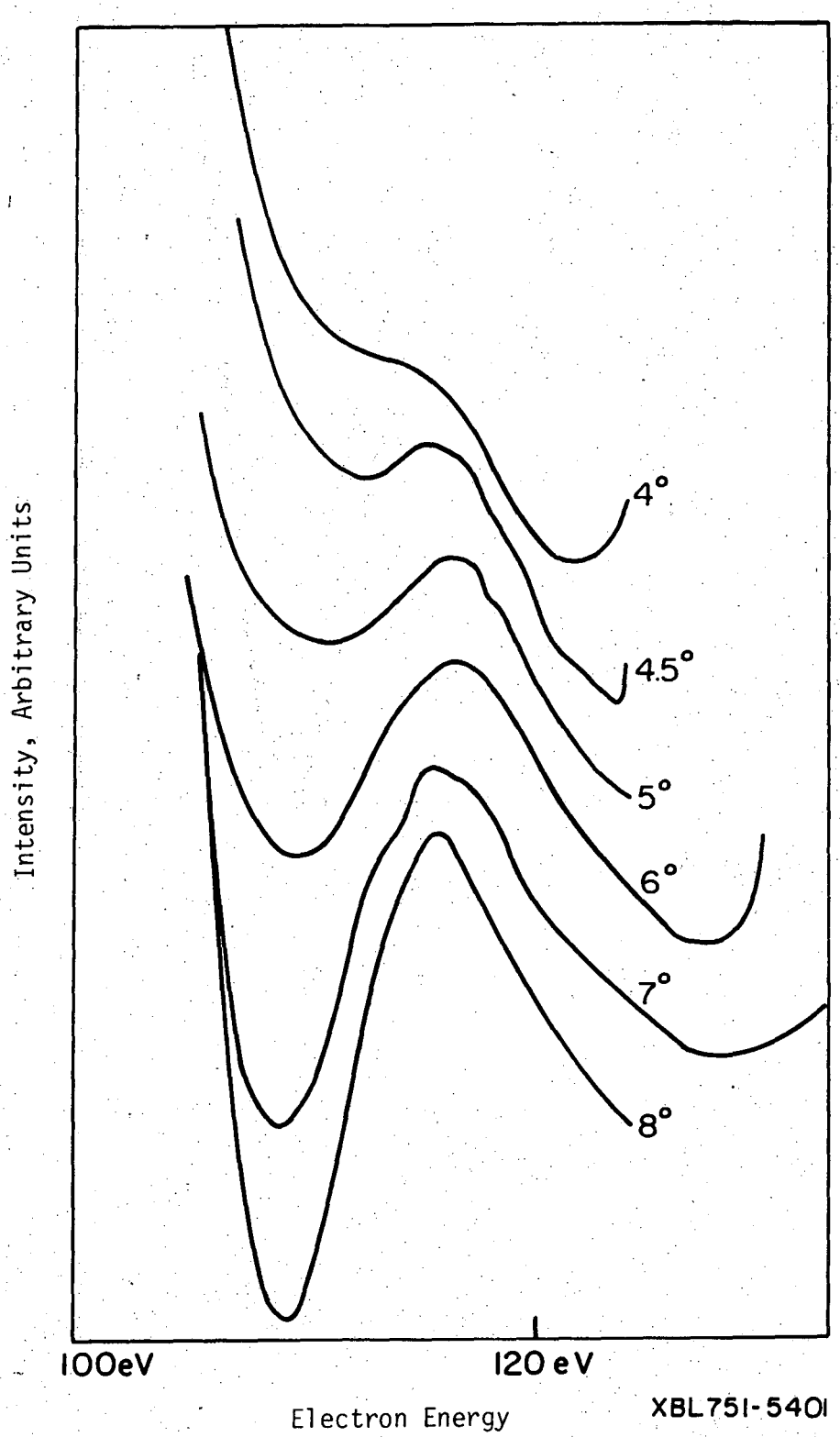

Fig. 9

SURFACE DEBYE TEMPERATURES

	Energy	52	96	117	137	256	325
Present Study	Θ_D	460°	480°	430°	410°	655°	---
	$\overline{u_\perp^2}^{1/2}$	0.81	0.75	0.87	0.91	0.57	---
Theeten et al.	Θ_D	---	460°	---	420	600	700
	$\overline{u_\perp^2}^{1/2}$	---	0.81	---	0.89	0.59	0.53

Bulk Values

$\Theta_D = 689°K$

$\overline{u^2}^{1/2} = 0.572$

Θ_D, °K

$\overline{u_\perp^2}^{1/2}$, Å$\times 10^2$

Fig. 10

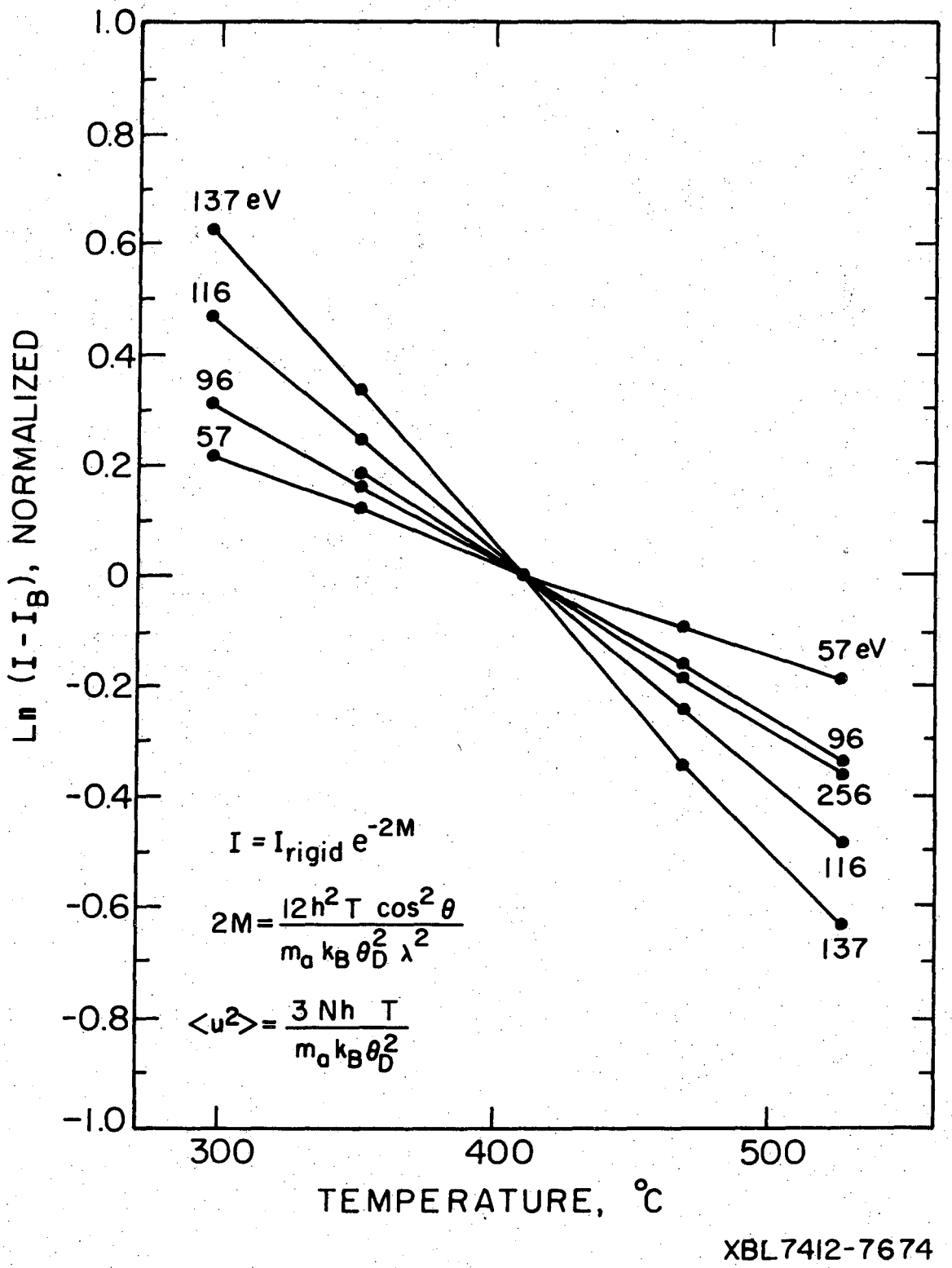

Fig. 11

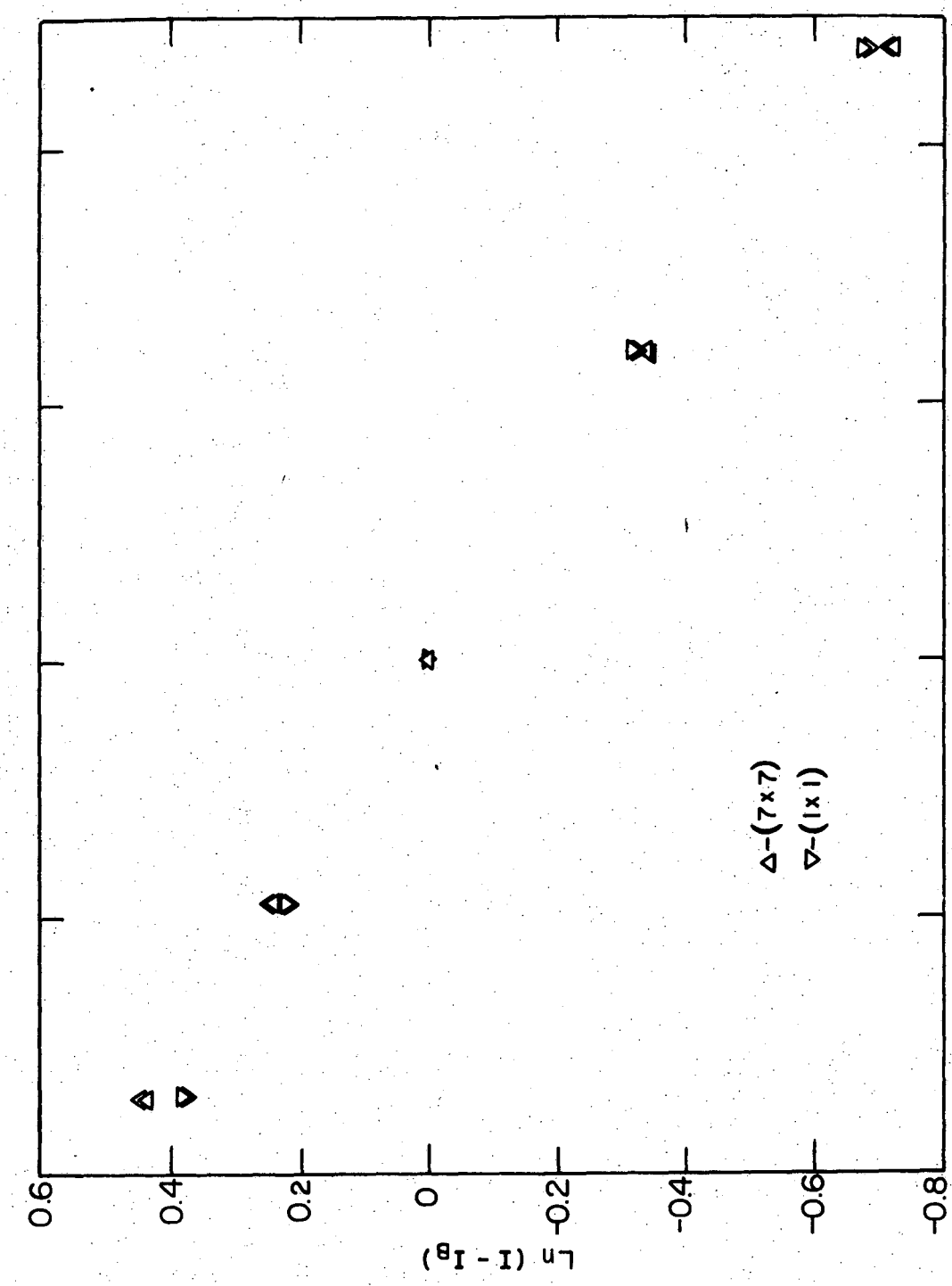

XBL 751-5532

Fig. 12

TECHNICAL INFORMATION DIVISION
LAWRENCE BERKELEY LABORATORY
UNIVERSITY OF CALIFORNIA
BERKELEY, CALIFORNIA 94720